

Harnessing intrinsic localized modes to identify impurities in nonlinear periodic systems

M. Thota, R. L. Harne, and K. W. Wang

Citation: [Journal of Applied Physics](#) **117**, 074505 (2015); doi: 10.1063/1.4913256

View online: <http://dx.doi.org/10.1063/1.4913256>

View Table of Contents: <http://scitation.aip.org/content/aip/journal/jap/117/7?ver=pdfcov>

Published by the [AIP Publishing](#)

Articles you may be interested in

[Dynamics of impurity attraction and repulsion of an intrinsic localized mode in a driven 1-D cantilever array](#)
Chaos **25**, 013103 (2015); 10.1063/1.4905254

[A study on bifurcations and structure of phase space concerning intrinsic localized modes in a nonlinear magneto-mechanical lattice](#)

AIP Conf. Proc. **1474**, 55 (2012); 10.1063/1.4749297

[Visualizing intrinsic localized modes with a nonlinear micromechanical array](#)

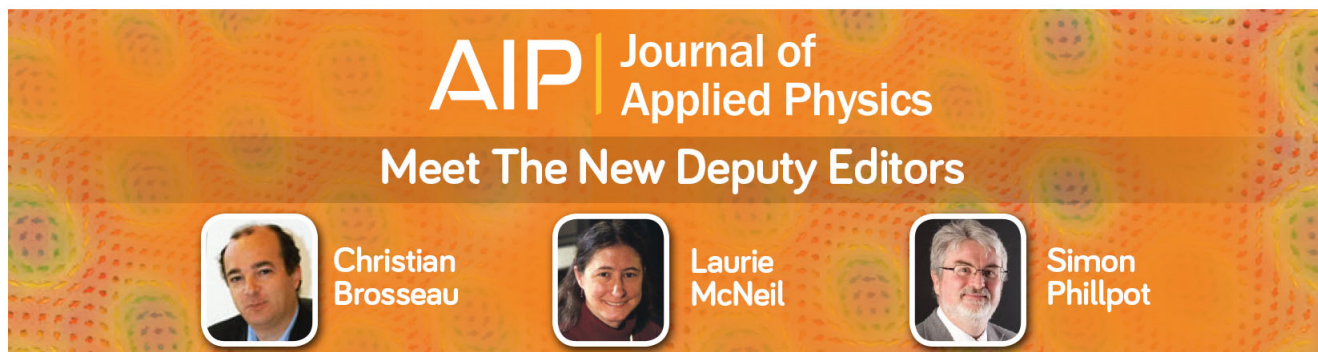
Low Temp. Phys. **34**, 543 (2008); 10.1063/1.2957286

[Introduction: Nonlinear localized modes](#)

Chaos **13**, 586 (2003); 10.1063/1.1577332

[Local vibrational modes of impurities in semiconductors](#)

J. Appl. Phys. **87**, 3593 (2000); 10.1063/1.372453

A promotional banner for the Journal of Applied Physics. It features the journal's logo at the top, followed by the text 'Meet The New Deputy Editors'. Below this, three circular headshots of the new deputy editors are shown, each with their name written to the right: Christian Brosseau, Laurie McNeil, and Simon Phillpot. The background of the banner is a vibrant, abstract pattern of orange, yellow, and green dots and swirls.

Harnessing intrinsic localized modes to identify impurities in nonlinear periodic systems

M. Thota, R. L. Harne,^{a)} and K. W. Wang

Department of Mechanical Engineering, University of Michigan, Ann Arbor, Michigan 48109, USA

(Received 30 October 2014; accepted 8 February 2015; published online 20 February 2015)

Intrinsic localized modes (ILMs) are concentrations of vibrational energy in periodic systems/lattices due to the combined influences of nonlinearity and discreteness. Moreover, ILMs can move within the system and may strongly interact with an impurity, such as a stiffness change, mass variation, etc. Numerous scientific fields have uncovered examples and evidence of ILMs, motivating a multidisciplinary pursuit to rigorously understand the underlying principles. In spite of the diverse technical studies, a characterization of ILM interaction behaviors with multiple impurities in dissipative lattices remains outstanding. The insights on such behaviors may be broadly useful when dynamic measurements are the only accessible features of the periodic system. For instance, one may guide an ILM within the lattice using a deliberately applied and steered impurity and harness the observed interaction behaviors with a second, static (immovable) impurity/defect to identify how the underlying lattice is different at the second, defected site, whether or not one knew the position of the defect *a priori*. In this spirit, this research studies, analyzes, and characterizes the interaction types amongst an ILM and multiple impurities, and devises a method to identify a static defect impurity using quantitatively and qualitatively distinct interaction phenomena. The method is found to be robust to moderate levels of lattice stiffness heterogeneity and is applicable to monitor various property changes that represent impurities. Finally, experimental studies verify that ILMs interact with multiple impurities in unique ways such that defect features may be effectively identified. © 2015 AIP Publishing LLC.

[<http://dx.doi.org/10.1063/1.4913256>]

I. INTRODUCTION

Intrinsic localized modes (ILMs) are areas of localized energy that occur in periodic arrays of discrete nonlinear oscillators when a sufficient level of energy is imparted into the lattice/system. Additionally, it has been found that ILMs may freely and continually propagate. In driven, dissipative lattices, an impurity (i.e., a parameter perturbation) may be applied to a lattice position sufficiently close to the original ILM position to strategically guide the localized energy from one pinned position to another. Such unique energy localization, propagation, and guiding have attracted multidisciplinary attention due to the many physical domains in which ILMs are realized.^{1–7} These include studies regarding anti-ferromagnets,⁸ cantilever arrays,^{9,10} electrical transmission lines,¹¹ and coupled pendula,¹² among other investigations in the optical, biological, and chemical sciences.^{13–15} Consequently, discoveries on the underlying principles of ILMs help to inform a broad spectrum of researchers. In particular, recent attention has been directed towards ILMs in the context of micro(electro)mechanical oscillator arrays, since lattices of many degrees-of-freedom may be readily fabricated with which to carefully probe the global dynamics for clear insights.^{7,16}

Since ILMs occur in periodic arrays, many efforts have examined the vulnerability of ILMs to impurities within the

system. In conservative lattices, propagating ILMs may be transmitted, trapped, or reflected at a fixed lattice impurity location based upon the difference between the oscillation frequency of the ILM and the frequency that characterizes the impurity mode.^{13,17,18} For dissipative lattices, pinned ILMs may be similarly affected based upon difference between the frequency of the driving excitation and the impurity mode frequency of a moving impurity.¹⁶ In both conservative and dissipative lattices, the softening or hardening nonlinearity and the linearized frequency spectrum govern whether a positive or negative difference in the aforementioned frequency pairs will lead to transmission, trapping, or reflection. Using these findings, methods have been devised to deliberately manipulate an ILM by introducing and steering an impurity near the ILM location.¹⁶

To date, the extent of such studies has been limited to interaction types between an ILM and a *single* impurity. Because of the nonlinearities and intricate localization characteristics involved, it is not viable to assume that interaction phenomena amongst ILMs and *multiple* impurities are fully represented by those occurring between an ILM and a *single* impurity. This is an important gap in the complete characterization of ILM behaviors because there may be a broad usefulness to leveraging the observable interaction dynamics. In particular, deliberately guiding an ILM with one impurity through the lattice provides a means, first, for energy localization (i.e., targeted interrogation), whereas the ILM interaction behavior with a second impurity could then be harnessed as a means for system identification. The net result

^{a)}Author to whom correspondence should be addressed. Electronic mail: rharne@umich.edu

could be a novel parameter identification strategy for complex nonlinear periodic systems that are only observed and understood through dynamic measurements.

The aims of this research are to elucidate the interaction behaviors amongst an ILM and multiple lattice impurities and to use the findings to formulate an effective methodology to identify defects in nonlinear periodic systems/lattices. Namely, the study examines the interaction of an ILM with multiple impurities, where a steered impurity guides the ILM within the system to ultimately intersect a lattice site possessing a second, immovable impurity representative of a defect about which some fundamental knowledge is sought, such as its magnitude and the corresponding lattice site position, and so on. While there are a variety of recent investigations on the guiding and/or localization of vibrational energy in periodic systems for the purposes of identifying the underlying structural properties,^{19–22} to date, ILMs have yet to be considered as a means to this end.

The following Secs. II and III detail the modeling development and present theoretical findings which are utilized to catalog the multiple, distinct interaction behaviors observed when an ILM contacts multiple impurities in the periodic array. The relations between detection capabilities and impurity characteristics are investigated in Sec. III through extensive model simulations, and lead to the formulation of a strategy which enables the identification of static lattice impurity location and strength. Next, the robustness of the identification approach to the addition of randomly distributed lattice stiffness heterogeneity is statistically examined. In Secs. IV and V a nonlinear periodic oscillator array is then fabricated and experimentally evaluated to verify the principles of the defect identification strategy. Finally, a brief summary of the key advancements made in this research is provided in Sec. VI.

II. MODEL FORMULATION AND EXAMINATION METHOD

To complement prior studies with the new insights regarding interactions amongst ILMs and multiple impurities, this research employs an established model of a multi-degree-of-freedom nonlinear oscillator array, previously developed by Sato *et al.*¹⁶ The model is shown in the schematic of Fig. 1 and is generalized such that it represents numerous realizations of nonlinear periodic lattices,^{23,24} including the experimental system considered here (to be detailed in Sec. IV). The periodic system examined by Sato *et al.*¹⁶ was a microelectromechanical cantilever array coupled via a small, under-etched silicon overhang. Deflection of one cantilever relative to a nearest neighbor deformed the overhang such that it induced linear and nonlinear restoring forces, modeled according to linear and cubic power terms of the overhang deformation. The inter-site stiffnesses provided by the overhang were modeled as primarily influential between a central oscillator and its six nearest neighbors in each direction along the lattice. Sato *et al.*¹⁶ determined that the six nearest neighbors approximation was sufficient to capture the salient dynamics observed experimentally once the corresponding inter-site coupling parameter values were identified through a model fitting

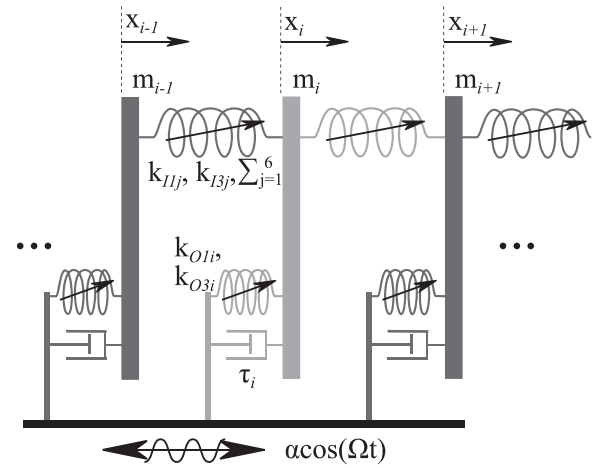


FIG. 1. Schematic of one-dimensional, lumped-parameter nonlinear oscillator array.

approach. For the present purposes of employing the model, the number of oscillators within the array (100) is selected to sufficiently minimize boundary condition influences on ILM behaviors within the system, but is otherwise arbitrarily chosen. The boundary conditions are non-periodic such that the first and last (100th) oscillators are not coupled. Periodic (i.e., cyclic) boundary conditions are known to simply circulate a moving ILM from one end of the array to the other, whereas non-periodic boundaries will reflect the ILM but not otherwise change the global behaviors involved with ILM propagation and pinning.^{7,17,25}

The governing equation of motion for the i th mass is¹⁶

$$m_i \ddot{x}_i + \frac{m_i}{\tau_i} \dot{x}_i + k_{O1i} x_i + k_{O3i} x_i^3 + \sum_{j=1}^6 (k_{I1j} (2x_i - x_{i-j} - x_{i+j}) + k_{I3j} ((x_i - x_{i-j})^3 + (x_i - x_{i+j})^3)) = m_i \alpha \cos(\Omega t). \quad (1)$$

Here, m_i is mass; τ_i is time constant; k_{O1i} (k_{O3i}) and k_{I1j} (k_{I3j}) are linear (cubic) stiffnesses of the i th oscillator and coupling spring, respectively, corresponding to on-site (O) and inter-site (I) effects; the summation of nearest neighbor restoring forces is taken over j ; α is acceleration amplitude; Ω is external driving frequency; and the overdot is differentiation with time t . This research employs the periodic system and excitation parameters that were previously selected in Ref. 16 for complementing the previous developments with the findings herein. Table I provides these values.

Technically, the original laser-heating strategy to induce impurities in the microcantilever array¹⁶ and the particular strategy employed in the experiments of this research influence both linear and nonlinear stiffness coefficients. However, to reduce the number of control variables being manipulated in the model, only local linear stiffness reduction was originally applied to account for impurities.¹⁶ Correspondingly, the theoretical work of this research applies on-site linear stiffness reduction to effect impurities within the lattice. Thus, all references hereafter to impurities indicate on-site linear stiffness reduction. Throughout the modeling studies presented below, the static impurity is introduced to the 40th oscillator while the deliberately

TABLE I. Model parameters. f_1 (f_2) and f_3 (f_4) are lowest (highest) frequencies of lower and upper bands of frequency spectrum of linearized system.

m_i (=odd), m_i (=even) (10^{-13} kg)	k_{Oli} (=odd), k_{Oli} (=even) (N/m)	k_{O3} (10^8 N/m ³)	$k_{I11-116}$ (N/m)
7.67, 6.98	0.102, 0.0976	1.00	0.104, 0.0405, 0.0189, 0.0118, 0.00887, 0.00346
$k_{I31-136}$ (10^{10} N/m ³)	τ (10^{-3} s)	f_1, f_2, f_3, f_4 (10^3 Hz)	t_p (10^{-6} s)
4.0, 0, 0, 0, 0, 0	8.75	59.0, 134.0, 139.0, 147.4	6.71

steered impurity location varies in time to manipulate the ILM position. For consistency, hereafter, the static impurity is referred to as the defect.

To generate the pinned ILM, the array begins with quiescent initial conditions and the frequency of the uniformly applied base excitation is increased linearly.^{3,16,26} As shown in Fig. 2(a), the array is harmonically driven starting at a frequency (147 kHz) which is lower than the highest frequency of the harmonic spectrum ($f_4 = 147.4$ kHz, see Table I), then ramped up linearly to 149.03 kHz in 2500 excitation periods t_p , and finally kept constant. Due to the amplitude of base acceleration α employed during the sweeping strategy, a modulational instability is induced and the uniform linear mode collapses, thereby presenting the opportunity for ILMs to form.¹¹ Rather than excitation frequency ramping, large and random initial conditions with a uniform driving, provided above f_4 , may trigger ILMs in nonlinear, dissipative lattices.³ On the other hand, the final pinning location(s) by this approach are less consistent from trial to trial since the strong nonlinearity of the system is sensitive to initial conditions. Therefore, this research employs the harmonically driven and ramped excitation style described above for more consistent generation of ILMs which, for a prescribed set of system and excitation parameters, produces identical results from one numerical simulation to the next. In this study, simulations are conducted with various steering and defect impurity stiffness changes (strengths) and the same excitation frequency profile, while the excitation amplitude α required to induce pinned ILMs slightly varies due to changing defect

strength which was recognized by past researchers.¹⁶ Throughout all simulations, the energy of each generated ILM was maintained,¹⁷ and, to this end, the standard deviation of all resultant ILM amplitudes was found to be two orders of magnitude less than the mean.

For an array possessing hard nonlinearity, utilizing an impurity mode *below* the highest frequency of the harmonic spectrum (f_4)—produced by a local, on-site linear stiffness reduction—will repel the pinned ILM away from the impurity location if it is near enough in the lattice to the ILM. Therefore, a strategy is devised to guide the ILM throughout the array to interact with the static defect. For example, as shown in Fig. 2(c), the defect is at site 40 (dotted line), while results from the simulation show that ILM is initially pinned at site 58 (the darkness of shading indicates an increased RMS of mass displacement). Thus, because the ILM will be repulsed from the impurity type employed here and in order to study the interaction behavior amongst the ILM and the two impurities, the steered impurity (thin solid line) is introduced to site 70 and is guided toward the ILM at a uniform rate towards the location of the defect. To avoid inducing additional influences into the investigation by steering an impurity at a rate comparable to that rate observed in the ILM propagation, the steering impurity is repositioned by one array site per 300 excitation periods t_p which is a sufficiently slow rate with respect to the observed ILM propagation. In the example shown in Fig. 2(c), upon first interacting with the guided impurity around a time of 10 000 excitation periods, the pinned ILM repels away from the steered impurity

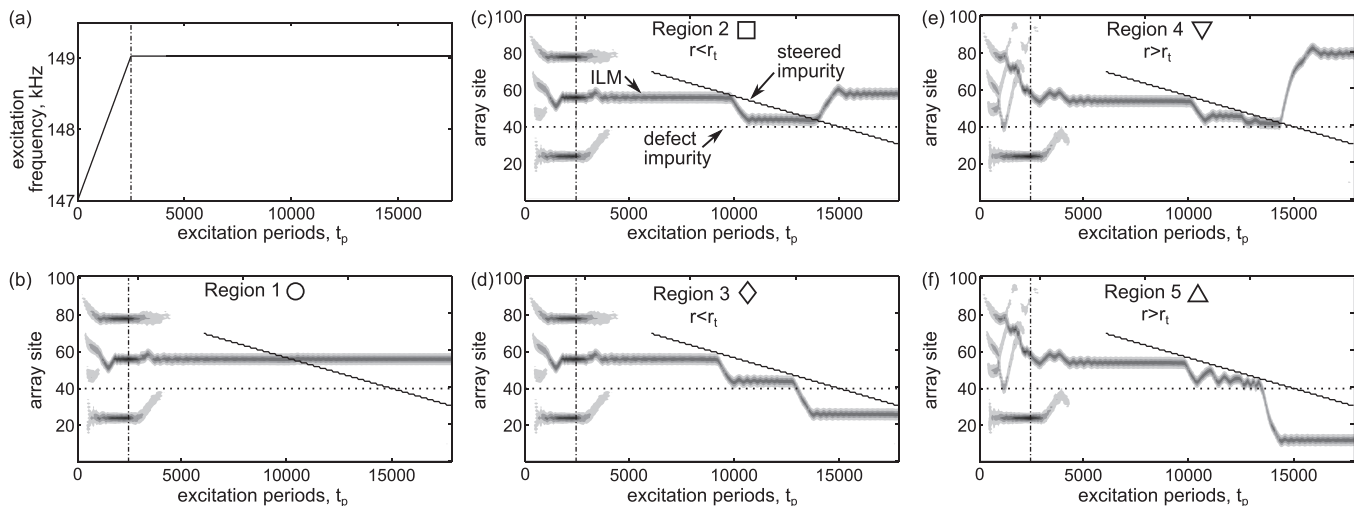


FIG. 2. (a) Excitation frequency sweep. Plots (b)–(f) show RMS of mass displacement over time for all 100 oscillators in the array. Dark regions indicate large displacements. An ILM is identified via persistence of large displacements over time. (b)–(f) Five classification types of ILM interactions with steered and defect impurities. In (b)–(f), the dashed–dotted curve is time at which excitation frequency ramp ends; the solid curve is steered impurity site; the dotted curve is the defect location.

location at a measurable rate r and then, in this scenario, pins to a different array location. Because different static defect strengths are employed, the ILM may initially pin to unique sites. Thus, while the ILM generation strategy used in this study is the same throughout all following simulated results, the guiding strategy changes based upon where the ILM became pinned. On the other hand, the steering rate for the impurity is selected to be at $1/300$ array sites per excitation period (~ 0.003 sites/ t_p) throughout the simulations. Finally, once it is generated, the simulations correspondingly compute the ILM propagation rate r , determined by tracking the peak response of the ILM over a given period of time, comparable to monitoring the propagation of a wave in the lattice.

III. MODEL STUDIES

A. Interaction types of an ILM with multiple impurities

The coupled nonlinear equations of motion for the 100-oscillator array, represented by Eq. (1), are numerically integrated using a fourth-order Runge–Kutta algorithm in MATLAB. The required integration tolerance, 10^{-10} , is set to a level that is 7 orders of magnitude smaller than the default because simulations showed sensitivity to levels around the default. Reducing the integration tolerance from the default led to steadily convergent simulation results, such that the level of 10^{-10} was even more refined than that required for consistency.

The simulations begin with the defect present, whereas the steered impurity is introduced only after the ILM is generated in consequence to the excitation style described in Sec. II. For each simulation, unique strengths are prescribed for the static defect and for the steering impurity. These values are varied over several orders of magnitude to broadly characterize the interaction behaviors amongst the ILM and impurities. Extending the parametric range of impurity strengths beyond that presented in the results below did not uncover additional unique interaction types. The full characterization across all defect and steering impurity strength parameters is conducted for a perfectly periodic array, as well as for two arrays that include distributed structural heterogeneity represented by an additional, random linear on-site stiffness variation δk_{Oli} , where the variation is randomly selected according to the ranges of $\delta k_{Oli} = [-0.075k_{Oli}, 0.075k_{Oli}]%$ or $\delta k_{Oli} = [-0.15k_{Oli}, 0.15k_{Oli}]%$. Such deviations from nominal values notably fall within the range of deliberately applied impurity strengths.

Each simulation (i.e., ILM behavior characterization) is considered to be complete once a sufficient number of excitation periods elapse after the steering impurity intersects the defect, providing ample time to characterize the potential reactions of the ILM. Thus, the exemplary results presented in Figs. 2(b)–2(f) show a substantial period of time elapsed following the intersection of moving and static impurities only for the sake of completeness. Note as well that the exemplary results in Figs. 2(b)–2(f) and 3 include different levels of defect impurity from the beginning of the simulations or different levels of steering impurity from the time at which the guided impurity is introduced; this explains the

unique transient characteristics that are observed in every case.

The identification of an interaction type is carried out based upon the ILM response due to the *steering impurity*, considering that one may not be aware of where a defect might be positioned within the lattice. In this way, one may infer from the interaction behavior more knowledge of the underlying nonlinear array by harnessing an identification strategy based upon the distinct dynamical behavior that is induced.

The following five distinct interaction types are observed in the simulations, and are quantitatively and qualitatively cataloged to assist in the formulation of a defect identification strategy. Representative time series of the interaction types are presented in Figs. 2(b)–2(f), where each type includes a corresponding symbol and Region number that is further utilized in Fig. 4.

Region 1. Fig. 2(b): The steered impurity does not perturb the ILM away from the location at which it was originally pinned.

Region 2. Fig. 2(c): The ILM repels over the steered impurity at a rate r less than a threshold rate r_t , $r < r_t$, and propagates in the direction opposite the steered impurity path.

Region 3. Fig. 2(d): The ILM is continually repelled from the steered impurity at rate $r < r_t$ in the direction of steered impurity path.

Region 4. Fig. 2(e): The ILM is repelled away from the steered impurity in the direction opposite the steered impurity path at a rate that temporarily exceeds the threshold rate $r > r_t$.

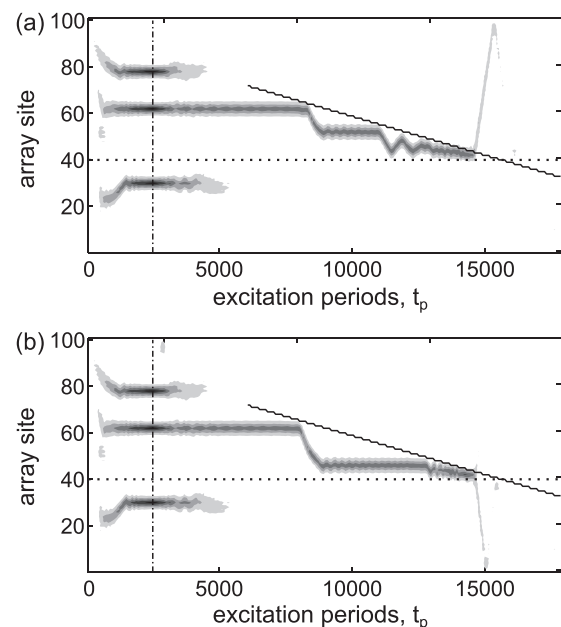


FIG. 3. RMS of mass displacement over time for all 100 oscillators in the array. Dark regions indicate large displacements. Plots (a) and (b) are representative cases of ILM annihilation such that the localized energy is propelled in a direction opposite or along with the steered impurity, respectively. These results are subsets of Regions 4 and 5, respectively. The plot conventions follow those of Fig. 2.

Region 5. Fig. 2(f): The ILM is repelled away from the steered impurity in the direction of steered impurity path at a rate that temporarily exceeds the threshold rate $r > r_t$.

Forming subsets of classification Regions 4 and 5, some simulations revealed complete ILM annihilation after the ILM encountered the steered impurity and the defect, as shown in Fig. 3. Yet, annihilation was not immediate following the impurity intersection, and the ILM would first propagate at rate $r > r_t$ prior to destabilization, which sufficiently satisfies the criteria related to either Regions 4 or 5. Much greater detail on the meaningful selection of a threshold ILM propagation rate is provided in the following Sec. III B.

The results of classifying the interaction behaviors from simulations utilizing the perfectly periodic array and the large range of steering impurity and static defect strengths are shown in Fig. 4. For brevity, the corresponding contour maps for the heterogeneous lattices are omitted, although the findings are comparable to those presented in Fig. 4. The distinct contour shading corresponds to the respective region number of an interaction behavior type, and the individual symbols plotted in Fig. 4 correspond to those provided in Figs. 2(b)–2(f). It is worth emphasizing that the demarcations amongst Regions in the figure are not influenced due to potential bias regarding the original site of ILM generation. As is described above regarding how the Regions are classified, the demarcations do not take into consideration the absolute position of the ILM, but rather the global behavior over the time elapsed from its generation to a sufficient period of excitation periods following the intersection of the steering impurity and static defect. In Sec. III B, the absolute position of the ILM is used as information to infer greater knowledge about the underlying nonlinear lattice and defect.

Figure 4 shows that Region 1, where the ILM is unaffected by the steered impurity, intuitively occurs when the steering impurity strength is insufficiently large to perturb the ILM from the initially pinned site, regardless of the

defect impurity strength. For greater values of the steering impurity strength, the ILM is able to be guided away from the originally pinned position. Under such conditions and for these system parameters, the ILM is observed to repel away from the steering impurity at a *nominal* propagation rate of around 0.01 array sites/ t_p when there is no additional interaction with a defect. Regions 2 and 3—that is, when the ILM is guided but does not exceed a threshold propagation rate r_t —are found to occur for different minimum values of steered and defect impurity strengths: $\sim 0.5\%$ defect strength for Region 2 and $\sim 1\%$ steering impurity strength for Region 3. This result is consistent when the array includes the additional, randomized structural heterogeneity (i.e., the random variation of ± 0.075 or 0.15% in on-site linear stiffness). Some results with and without stiffness heterogeneity indicated the minimum defect impurity strength required to classify the interaction phenomenon as Region 2 was as low as 0.05%. These findings suggest that ILMs are more influenced by static impurities when there is an intersection of dynamic and static impurities that may potentially trap the moving ILM at the intersection.

In terms of formulating an identification methodology for defects within the periodic structure, guiding an ILM and observing its repelling forward or backward across the steered impurity path is not of itself a viable indicator to determine the defect location or strength. Additional means of evaluating the phenomenological behaviors are required. To this end, a *threshold* ILM propagation rate r_t is introduced. The threshold rate enables a means to differentiate the many cases for which the ILM is, in fact, effectively steered, and thus helps to distinguish Regions 2 and 3 from Regions 4 and 5, respectively. In other words, Regions 2(3) and 4(5) represent qualitatively similar interaction behaviors, but in Region 4(5), the dynamic propagation of the ILM (as it repels from the steering impurity influence) exceeds a threshold r_t . The threshold rate used to plot Fig. 4 is $r_t = 0.05$ sites/ t_p . This rate is selected to be much greater than the nominal propagation rate ~ 0.01 sites/ t_p , and is greater still than the steered impurity rate ~ 0.003 sites/ t_p . A detailed description of the appropriate selection of this rate is presented in Sec. III B.

The upper-right quadrant of Fig. 4 is the principal parametric area (larger impurity and defect strengths) in which Regions 4 and 5 occur. For the threshold rate $r_t = 0.05$ sites/ t_p , the minimum range of defect impurity strength for which Region 4 occurs is approximately 2% which is comparable to the minimum steered impurity strength needed to observe phenomena of Region 5. These magnitudes of guided and static impurities are seen to be dependent upon the selection of the threshold rate on ILM propagation: for example, reducing the threshold reduces the minimum impurity strengths required to differentiate Regions 2 and 3 from Regions 4 and 5, respectively. From the simulations conducted with additional random structural heterogeneity, these demarcation boundaries are also found to be mildly affected by the random stiffness deviations considered here, which is consistent with prior findings that the relative effect of impurities on ILMs is governed by local as well as global lattice parameters.^{16–18,25}

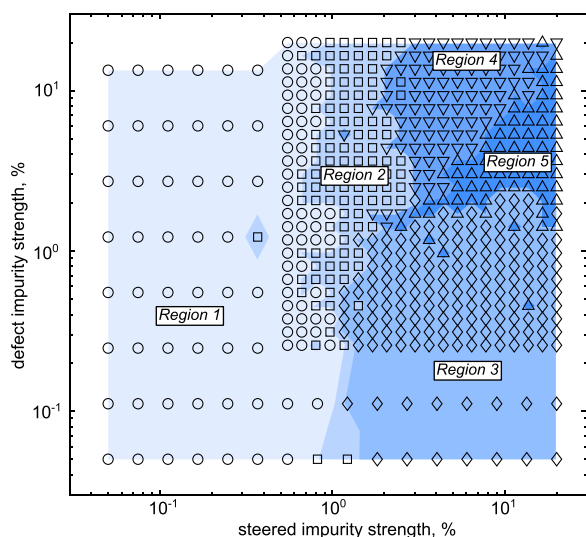


FIG. 4. ILM interaction behaviors with steered impurity and defect impurity, threshold rate $r_t = 0.05$ sites/excitation period t_p . Symbols and region numbers correspond to the ILM behaviors illustrated in Fig. 2 and described in the main text.

B. Determination of a threshold ILM propagation rate and assessment of defect detection robustness

Importantly, by the differentiation of Regions 4 and 5, a useful strategy may be established to infer additional information about the presence of a static defect within the non-linear array. Figure 5 illustrates the important connections uncovered between the ILM interaction behaviors and the number and location of results that are catalogued within Regions 4 and 5 as the threshold rate is varied. Each bar plot shows the percentage occurrence of oscillator array site at which the ILM propagation rate first exceeds the threshold. From Figs. 5(a) to 5(f), the selection for threshold rate increases from 0.02 to 0.07 sites/ t_p in 0.01 increments. Using a threshold of only 0.02 sites/ t_p which is just twice the nominal rate (~ 0.01 sites/ t_p), Fig. 5(a) shows that the propagating ILM exceeds the defined threshold for a large proportion (over 77%) of the simulations, and oftentimes exceeds the threshold close to the original site of steering. For example, a concentrated distribution of occurrences is observed around site 58, which—Figs. 2 and 3 show—was one common region for ILM generation. Therefore, the low threshold rate setting of $r_t = 0.02$ sites/ t_p does not present useful information about the defected site because the low value is frequently exceeded during the transient period that occurs after initially guiding the ILM away from a pinned position, regardless of the location of the original pinned site.

However, the results change dramatically in two ways for selections of threshold rate from 0.03 to 0.05 sites/ t_p . First, the total number of occurrences drops substantially suggesting that the threshold does indeed demarcate a quantitatively unique type of interaction behavior. Second, an apparent concentration of the occurrences develops around the actual defect site 40. For example, Fig. 5(b) shows that utilizing the threshold rate of $r_t = 0.03$ sites/ t_p leads to 23.0% of occurrences exceeding the threshold at the 38th array site, where the corresponding percentage is 34.5% for the threshold of 0.05 sites/ t_p , Fig. 5(d). As the threshold rate is increased to 0.06 sites/ t_p and greater, the concentrated distribution of the percentage of occurrences diffuses, no longer providing a meaningful link between the occurrences and the position within the array at which the defect is located. Interestingly, Fig. 5 shows that these results are very consistent when stiffness heterogeneity is introduced throughout the lattice. Even with a randomized linear stiffness deviation of $\pm 0.15\%$, the overall trends shown in Fig. 5 are comparable to those for the perfectly periodic array. All together, the results of Figs. 5 and 4 (along with corresponding, omitted contours for the heterogeneous lattices) show that a selection of the threshold rate of ILM propagation several times greater than the nominal rate enables one to identify whether and where a static defect in the array may be, and that the defect strength will be $\geq 2\%$ reduction in the local linear stiffness for the system parameters employed here.

When the threshold rate is set in the range of 0.03–0.05 sites/ t_p , a close inspection of individual simulation results reveals two explanations for the difference between the defect site 40 and the most identified site where the ILM rate first exceeds the threshold. First, it is found that when the

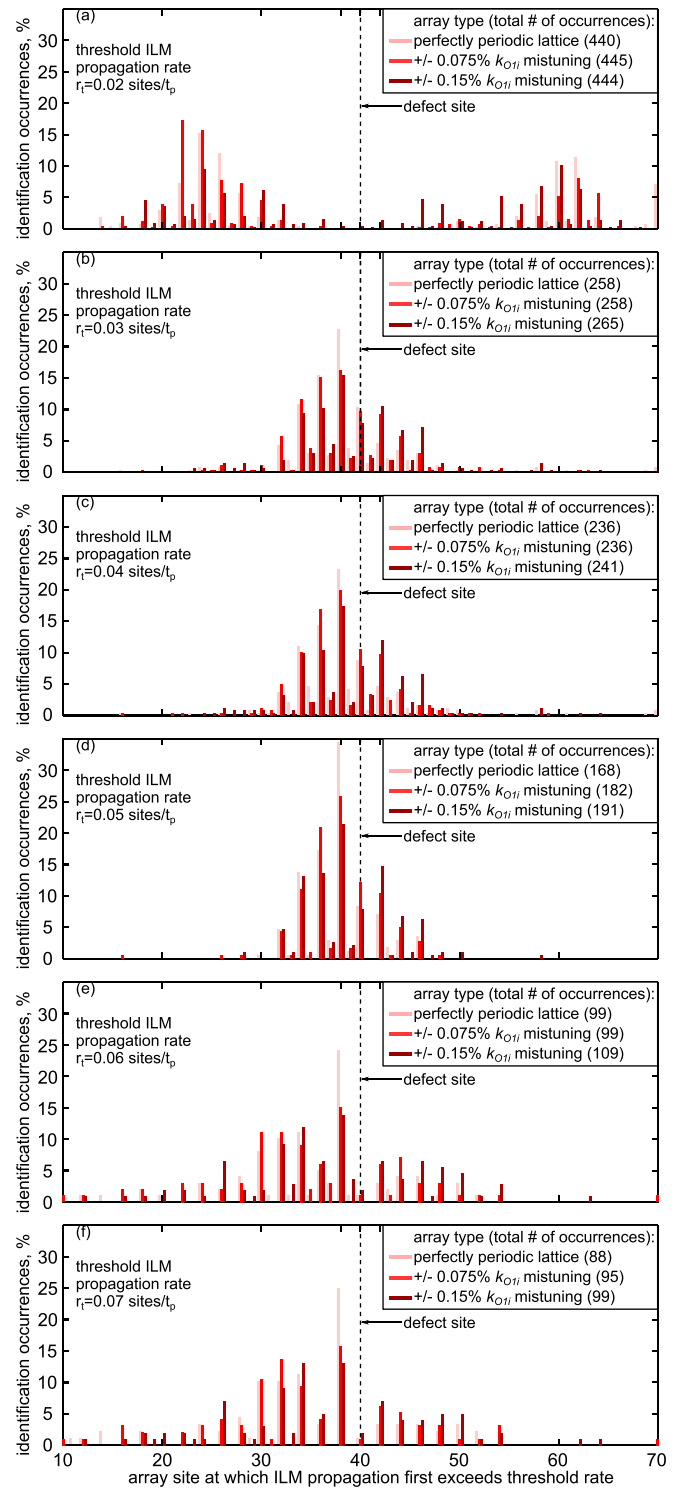


FIG. 5. Percentage of defect impurity site identification occurrences for threshold ILM propagation rates r_t of (a) 0.02, (b) 0.03, (c) 0.04, (d) 0.05, (e) 0.06, and (f) 0.07 array sites per excitation period t_p .

ILM rapidly repels *backward* across the steered impurity path, the ILM does not often reside at the site of the defect prior to repelling; thus, there are few opportunities to correctly identify site 40 for interactions classified by Region 4, and instead, site 38 is commonly the location where the ILM rate surpasses the threshold. Second, when the ILM is propelled *forward* across the defect site in the direction of the

steered impurity path (Region 5), it is found that it gradually accelerates away from site 40; therefore, it may not exceed the threshold rate while crossing the static defect impurity site and instead, site 42 is often the position where the ILM rate surpasses the threshold. In summary, conducting several examinations using incrementally increasing steering impurity strength that first repel the ILM *backward* and then *forward* at rates that exceed the threshold, a distribution of occurrences having a mean close to the defect position is produced, such as Fig. 5(c), giving a statistical basis with which to infer the true defect location.

Using the findings reported above, a lattice defect identification strategy is summarized as follows. First, a nominal rate of ILM propagation is identified, where the propagation rates are determined by tracking the peak response of the ILM over time, similarly as one would characterize the speed of a wave traveling through the lattice. The *nominal* rate is the rate at which the ILM propagates when perturbed from the originally pinned site using the smallest strength of steering impurity sufficient to this task. Then, a *threshold* rate of ILM propagation r_t is selected which should be several times greater than the nominal rate. As uncovered above, a useful value for the threshold may be selected from 3 to 5 times the nominal rate, for the system parameters considered here. Consequently, the findings from the extensive examinations conducted on the perfectly periodic and heterogeneous periodic arrays, as collected into Fig. 5, suggest approximate *lower* and *upper* limits for an appropriate selection of the threshold rate r_t . Then, repeated examinations of the structure using steered ILMs (with different level of steering impurity strength per evaluation) and observations of the positions at which the ILM propagation first exceeded the threshold rate will lead to a distribution of occurrences of these critical positions. From this distribution, as evidenced in Figs. 5(b)–5(d) for the suitable selections of the threshold rate, one may infer the defect is located near to the distribution mean. While the identification strategy described above is sufficient to identify linear stiffness reduction defects embedded in the nonlinear lattice studied here, the selection of the threshold rate of ILM propagation is subject to the composition of the lattice under consideration. Thus, the overall strategy may serve as a general guide for the development of useful lattice defect identification methods which may then specifically tailor the threshold rate value (like that explored in Fig. 5) to maximize identification effectiveness.

IV. EXPERIMENTAL SYSTEM PLATFORM

To verify the proposed approach for exploiting the interaction behaviors between an ILM and impurities for identifying defects in a nonlinear periodic system, a series of experimental efforts are conducted. A nonlinear periodic oscillator array is fabricated, as shown in Fig. 6. The array consists of 12 spring steel cantilever beams (Fig. 6 label A) which are coupled together through a continuous, spring steel coupling beam (label B). The attachment position and geometric deformation of the coupling beam between two cantilevers are comparable to the silicon overhang and corresponding deformation encountered with the microcantilever

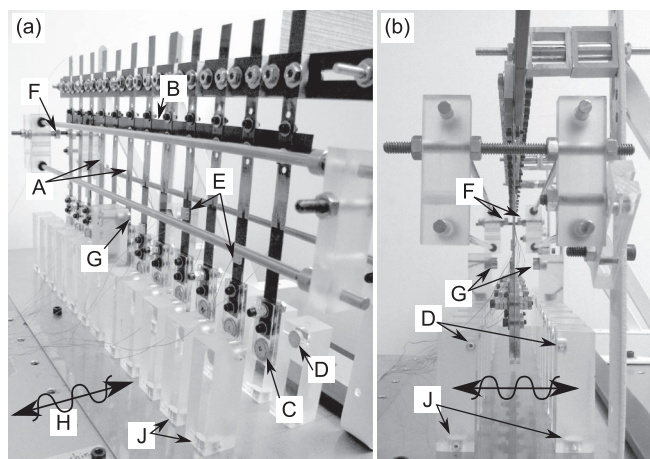


FIG. 6. Experimental platform. In (a) are shown the 12 unit array of (A) diatomic cantilever beams coupled together via a (B) continuous coupling beam. On-site hardening nonlinearity is induced using (C) a magnet at the beam tip and (D) magnets polarized so as to repulse the beam tip magnet. (F) A steering impurity composed of two attractive magnets is guided along rails while (G) a static/defect impurity is induced via two, fixed attractive magnets. (H) An electrodynamic shaker excites the system in the direction shown by the double arrow. The PZT patches are attached to the cantilevers on the opposite surfaces as those visible in (a). Each repulsive magnet PMMA block (D) is strongly fixed to the moving reference frame of the base due to the contact between a stainless steel plate base and (J) a supporting magnet.

array¹⁶ around which the generalized model was developed, as described in detail in Sec. II. The experimental boundary conditions are non-periodic, in agreement with the model composition. While non-periodic boundary conditions reflect a propagating ILM back into the lattice, periodic boundaries enable the circulation of a propagating ILM from one end of the lattice to the other, but do not otherwise change the global dynamic features regarding ILM propagation with respect to the non-periodic boundaries.⁷ Thus, experimental observations presented here are also relevant for global behaviors that occur for nonlinear lattices having periodic boundary conditions.

The local on-site stiffness nonlinearities are induced via magnetic interactions. A magnet (Applied Magnets ND033) is attached to each cantilever free tip (label C) which interacts with two repulsive magnets embedded in PMMA blocks (label D) that are spaced equal distances from the beam tip. These magnetic interactions induce a local hardening stiffness nonlinearity that is governed in magnitude based upon the distance between the magnets.²⁷ To more accurately achieve periodicity within the array, small magnetic masses (label E) (Applied Magnets NB001-N48) are attached to some cantilevers to counterbalance minor deviations in the observed local resonances. The PMMA blocks containing the magnets that induce local nonlinearities (label D) are attached to a stainless steel plate using additional magnets (label J) embedded at the other ends of the blocks.

Impurities are induced using the attractive interactions of the ferromagnetic spring steel cantilevers and additional magnets embedded in PMMA blocks. Such influences reduce the net restoring forces acting on the local cantilever at which the impurity is positioned (comparable to the

softening stiffness impurity type employed in the model), to the point that bistability may be induced under conditions that are not explored here.^{28,29} Two steered impurities (label F) move along rail guides to symmetrically influence a cantilever as the impurities pass an array site. The strength of the steered impurities is governed by the gap between these magnets and the ferromagnetic cantilevers. A fixed static/defect impurity (label G) is induced using two magnets which are fixed to certain positions with the array, and likewise, the distance between these magnets and the ferromagnetic cantilevers governs the resulting defect strength. The experimental system and bottom stainless steel plate are mounted to an electrodynamic shaker (label H) (APS Dynamics 400) which is excited in the direction indicated by the double arrows in Fig. 6.

Measurements of the exciting base acceleration are made using an accelerometer (PCB 352 C33). A lead zirconate titanate piezoelectric (PZT) patch (Piezo Systems T110-A4E-602) is bonded to the surface of each cantilever near the clamp using non-conductive cyanoacrylate. To initially determine the magnitude of a given cantilever beam velocity using the measured open-circuit voltage of the PZT strained by that cantilever, the following procedure is conducted. First, the array is excited at very low amplitude using a waveform of single frequency sufficiently less than the lowest linear modal frequency of the system. A laser interferometer (Polytec OFV 3001 S, OFV 303) measures each cantilever motion in consequence to the excitation while the corresponding PZT voltages are recorded. Then, the sensitivity of each PZT to the corresponding cantilever is determined to relate the measured voltage to the amplitude of the cantilever beam tip velocity. All relevant parameters of the experimental platform are provided in Table II. These parameters, and the descriptions given above, can be used in future investigations for model validation using the procedure described in the Appendix of Ref. 16 that presents the transformation of the continuum system parameters to those employed in the discretized model.

V. EXPERIMENTAL STUDIES

A. ILM generation

A large number of experiments are conducted to examine all of the salient features uncovered from the theoretical work regarding the generation of ILMs and the dynamic behaviors exhibited upon interaction with impurities. Similar

to the modeling investigations, for every experimental trial, an ILM is generated by a modulational instability due to the excitation frequency profile shown in Fig. 7(a). The excitation sweep begins at a frequency less than the highest harmonic modal frequency of the optic band (f_4) and is ramped up at a linear rate to 3.35% more than f_4 , after which time the excitation maintains a frequency of 1.0335 times f_4 . Due to this excitation strategy, applicable to the hardening lattice examined here, the uniform linear mode collapses (based upon the levels of base acceleration utilized) and ILMs may be formed. Exemplary cases are shown in Figs. 7(b)–7(f). In these sub-figures, the darkness of the shading indicates larger values of mean square cantilever velocity, and thus, concentrated dark areas over time indicate the persistence of an ILM at a given array site. As observed in Figs. 7(b)–7(f), the ILMs are generated on the even-numbered sites of the array, which is in agreement with the theoretical results; this finding is due to the di-atomic lattice composition. Figures 7(b)–7(f) clearly indicate that generation of ILMs in the experimental system is a robust procedure. In other words, throughout experimentation, an ILM is able to be generated at any of the even-numbered sites within the array. As a result, even though the same excitation profile is used throughout all experiments, unique results may be obtained regarding where the ILM finally becomes pinned. Note that the final ILM pinning location(s) is (are) due to a combination of initial conditions and the presence of static defects. These factors collectively explain the different global behaviors observed regarding the consistency of pinning an ILM at a precise location shown in Figs. 2(b)–2(f) (which included a static defect and had precise control over initial conditions) with those shown in Figs. 7(b)–7(f) (which do not include a static defect and have much less control over the initial conditions).

B. ILM interaction with a steered impurity

The size of the experimental oscillator array is found to be sufficient for steering and re-pinning of the ILM to new locations within the periodic system. One example case of this is shown in Fig. 8, where the steering impurity (attractive magnet pair moving along guide rails, label F in Fig. 6) approaches the ILM at array site 6 and causes the ILM to repel away and re-pin at site 4. Once transients behaviors have sufficiently decayed, the steered impurity continues toward site 4, at which point the ILM is repelled in the opposite direction as that in which the steering impurity travels,

TABLE II. Parameters of the experimental system. f_1 (f_2) and f_3 (f_4) are lowest (highest) frequencies of lower and upper bands of frequency spectrum of the system excited so as to induce only linear oscillations. l , w , and t are the length, width, and thickness of the beam. p is the distance between the clamped end of the cantilever beams and the attachment position of the coupling beam. Span m is the distance between adjacent unit cells, while span n is the distance between the hardening magnets. t_p is the period of the final constant-frequency excitation. The stand-off distances of the static/defect and steering impurities to the clamped end of the cantilever are provided.

m_i ($=\text{odd}$), m_i ($=\text{even}$) (kg)	cantilever beam (l , w , t) (mm)	coupling beam (w , t , p) (mm)		PZT length/width, thickness (mm)	
0.032, 0.026	152.4, 12.7, 0.508	12.7, 0.254, 25.4		6.35, 0.267	
defect impurity stand-off (mm)	steering impurity stand-off (mm)	span (m , n) (mm)	t_p (s)	f_1, f_2, f_3, f_4 (Hz)	
111.125	50.8	38.1, 50.8	0.055	14.5, 15.9, 16.5, 17.6	

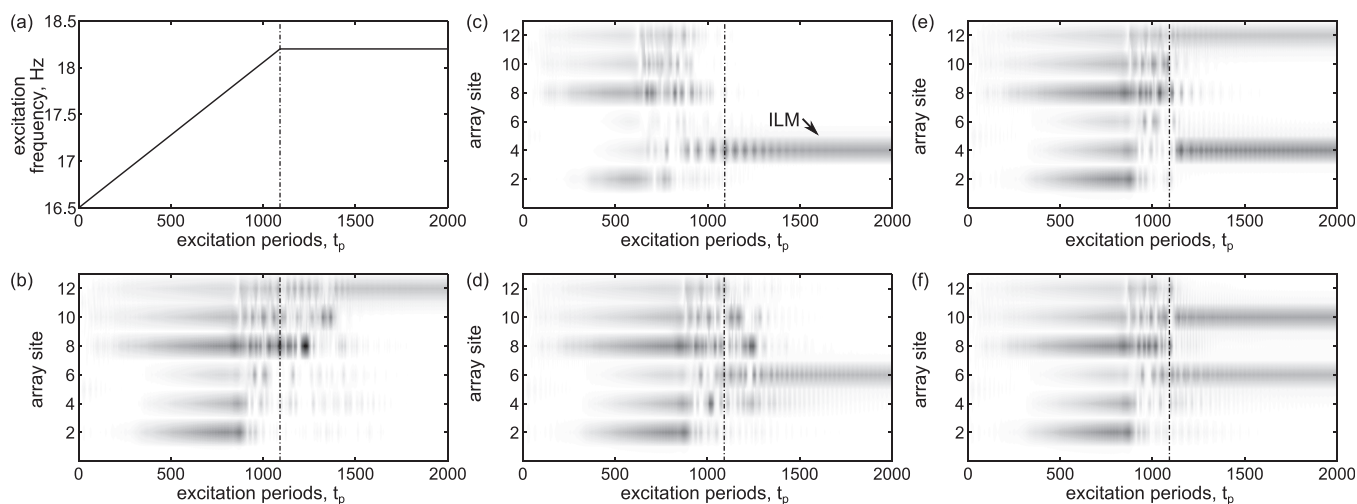


FIG. 7. (a) Excitation frequency profile imposed upon the array. In (b)–(f) are plotted the instantaneous mean square velocities of the cantilevers as a function of the time (in excitation periods) and according to array location. Darker shading of the contours indicates larger mean square velocities and thus localized energy. In (b)–(d), a single ILM is formed. In (e) and (f), two ILMs are formed.

and thus re-pins at site 6. The steering impurity continues through the array, reverses direction, and approaches the ILM at site 6. Upon interaction, the ILM is annihilated. This example shows—and an extensive number of trials found—that the current experimental system exhibits directionality dependence in terms of the ability to steer ILMs within the array. In other words, steering and re-pinning of ILMs is successful with steered impurities traveling from higher to lower values of array site number.

C. ILM interaction with multiple impurities

Additionally, in all experimental trials that successfully steered an ILM, the ILM is observed to jump two sites away from the original location, whether or not a static defect was present. In terms of verifying the proposed defect identification strategy, this result may be limiting since the ILM does not propagate far enough to enable a confident quantification

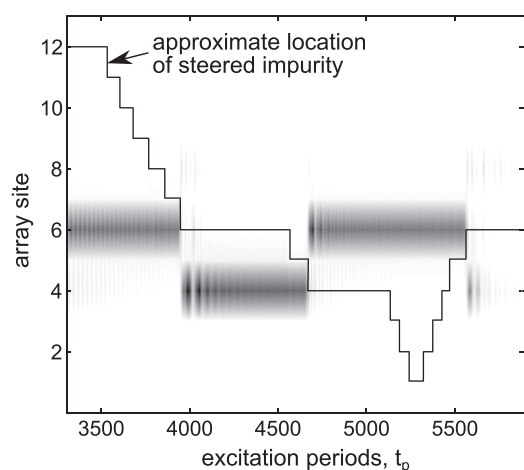


FIG. 8. Instantaneous mean square velocities of the cantilevers as a function of the time (in excitation periods) and according to array location. Darker shading of the contours indicates larger mean square velocities and thus localized energy. An ILM is steered from site 6 to 4 and then back to 6. The steering impurity annihilates the ILM when it approaches the pinned ILM location from the opposite direction.

of propagation rate. Thus, an alternative means to evaluate ILM propagation rates for the experimental system is devised.

The procedure begins similarly to that employed in the model: a static/defect impurity is positioned at a site within the array and remains in this location throughout the experiments. The defect is placed at site 6 in the array. Then, the excitation is applied to induce the modulation instability which leads to the generation of one or more ILMs. To enhance the consistency of the conclusions, the data post-processing only evaluates experimental results for which one ILM was generated, while other scenarios are omitted from consideration. Under these conditions, it was found that a single ILM would occur at array site 12. The repeatability in achieving this pinning location is in qualitative agreement with the theoretical finding that the number of potential ILM pinning sites is significantly reduced when the excitation begins with a defect positioned in the lattice. Experimentally, once the ILM is sufficiently pinned to site 12, a steering impurity approaches site 12 from a position external to the array to cause the ILM to repel away. The guide rails supporting the steering impurity extend sufficiently beyond the lattice boundary conditions to enable a consistent approach from the external position. The resulting propagation of the ILM is observed to be very fast in terms of the size of the array, such that an initial inspection of instantaneous cantilever dynamics shows quickly reflecting paths of high energy, like that seen in Fig. 9.

As a result, the rate of ILM propagation is more clearly identified using the first path of localized energy upon interaction with the steered impurity. Such paths are identified by the dashed–dotted lines in the example cases shown in Fig. 9 for (a) smaller and (b) greater steering impurity strengths. Many such experimental trials are conducted, and the mean and standard deviation of the measured ILM propagation rates are presented in Table III. It is seen that the ILM propagates at a faster rate when the steering impurity has a larger strength, more than 2.5 times faster than for the smaller steering impurity strength. In addition, Fig. 9 shows that for either level of steering impurity strength, the ILM does not

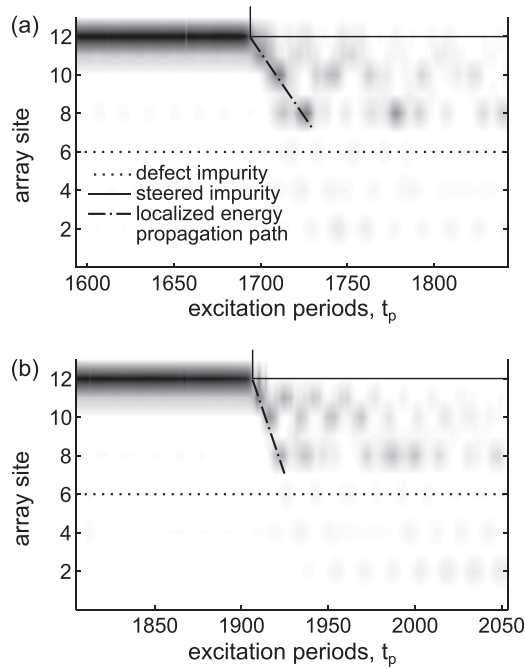


FIG. 9. Instantaneous mean square velocities of the cantilevers as a function of the time (in excitation periods) and according to array location. Darker shading of the contours indicates larger mean square velocities and thus localized energy. Dotted/solid lines represent defect/steered impurity positions, respectively; the dashed–dotted lines represent the propagation path of the ILM upon interaction with steered impurity. In (a) are shown experimental measurements for the smaller steered impurity strength, and in (b) are results for the greater steered impurity strength.

propagate beyond the location of the defect impurity. A significant portion of the energy is shown to remain confined within the array from site 7–12, providing a demarcation line at site 6 that suggests to an external observer that something is at this array location preventing the passage of energy throughout the periodic system.

The experimental calculations of the ILM propagation rate, shown in Table III, are determined from the data acquired *before* the first reflection of the ILM against the defect position. Due to the limitations imposed by the size of the experimental lattice, the prior evaluation of ILM propagation rate is slightly different than the proposed protocol described in Sec. III B, which identified the rate *after* the first reflection. Thus, to validate these results, the model is utilized again to emulate the conditions encountered by the present experimental system. Some exemplary results from these numerical studies are presented in Fig. 10. In the additional simulations, the nonlinear periodic array has a static defect impurity at site 40 while a steering impurity approaches from sites numbered higher than this value. An ILM is ultimately pinned to site 48 at the time when the steered impurity interacts with it. Simulations are conducted for smaller and greater steering impurity strengths, as shown in Figs. 10(a) and 10(b),

TABLE III. Experimental results of mean ILM propagation rate.

ILM propagation rate (sites/ t_p)	Mean	Standard deviation
Weak impurity	0.129	0.007
Strong Impurity	0.339	0.012

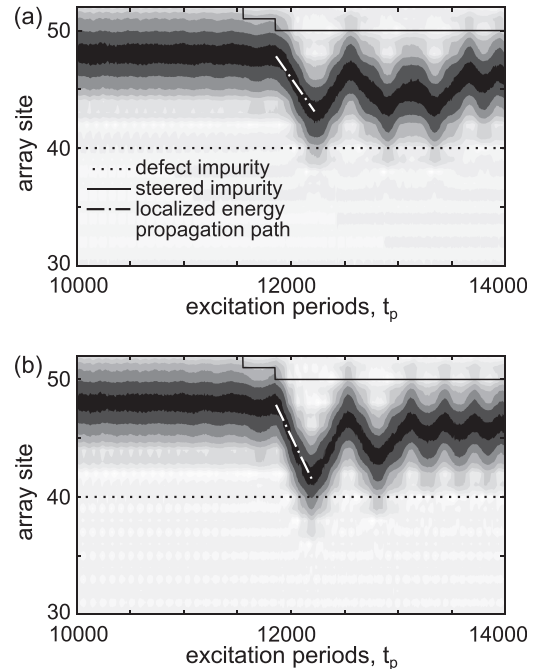


FIG. 10. Instantaneous root mean square displacements of the oscillators as a function of the time (in excitation periods) and according to array location. Darker shading of the contours indicates larger root mean square displacements and thus localized energy. Dotted/solid lines represent defect/steered impurity positions, respectively; the dashed–dotted lines represent the propagation path of the ILM upon interaction with steered impurity. In (a) are shown numerically simulated results for the smaller steered impurity strength, and in (b) are results for the greater steered impurity strength.

respectively, while the strength of the static defect remains constant, thus emulating the experimental conditions. Figure 10 shows that the greater steering impurity strength leads to faster ILM propagation rates immediately upon interaction between the steered impurity and ILM -0.02 sites/ t_p as compared to 0.013 sites/ t_p for smaller steered impurity strength. Additionally, the energy of the ILM remains trapped and continually reflecting back-and-forth between the static/defect and fixed steering impurity positions within the periodic array, and does not propagate forward to array sites numbered less than the defect position.

Each of these additional numerical findings—repeated reflection of the ILM between the steered and defect impurities, faster ILM propagation rates upon initial encounter with the steering impurity, and prevention of ILM energy from passing the defect array site—are qualitatively very similar to the experimental findings. The good agreement between theoretical and experimental observations additionally indicates that the experimental array, although smaller in number of oscillators from one end of the lattice to the other, provides for a useful means to reproduce the salient dynamical behaviors that occur amongst an ILM and multiple impurities. Moreover, the results provide a decisive verification of the defect identification strategy and extend the confidence in the predictive capabilities of the model formulation.

VI. SUMMARY

This research investigates the interaction phenomena that occur amongst multiple impurities (local linear stiffness

reductions) and a moving ILM in a nonlinear periodic oscillator array. Five distinct interaction types are discovered and differentiated, thereby introducing the opportunity to identify features of the impurities by a quantitative and qualitative characterization of the ILM behavior as it propagates through the lattice. It is revealed that a sudden increase in the ILM propagation rate may be used to identify the location and magnitude of a defect (immovable impurity), although the onset of the ILM acceleration may not necessarily occur at the defect site itself. On the other hand, it is found that repeated examinations of the lattice with differing levels of steering impurity strength will produce a distribution of critical sites at which the ILM exceeds a selected threshold rate of ILM propagation, and that the mean of this distribution is very near to the actual defected, static impurity position. The findings also reveal that stiffness heterogeneity throughout the periodic array, as great as a randomized 0.15% linear stiffness change, does not significantly affect identification results. In contrast, the threshold ILM propagation rate, chosen to distinguish the interaction behaviors, clearly regulates the confidence that the site of sudden ILM acceleration will correctly correspond to the defect site. Fortunately, lower and upper limits on the selection of a threshold rate provide an intelligent means with which to choose an appropriate value that improves the accuracy of identifying the defect position. Experimental studies conclusively show that an ILM uniquely propagates through a periodic structure based upon the strengths and locations of multiple impurities, serving to verify the theoretical observations. The good qualitative agreement between modeling and experimentation also enhances the confidence of the predictive capabilities of the model, including towards the determination of an effective threshold ILM propagation rate for the defect identification strategy. Due to the numerous sciences in which ILMs have been investigated, these results present useful means to characterize impurities in nonlinear lattice when dynamic measurements are the only accessible features of the system. Thus, the findings of this research may inform and guide a broad variety of future applications to harness the underlying physics of ILMs and multiple lattice impurities.

ACKNOWLEDGMENTS

This research was supported by the National Science Foundation under Award No. 1232436.

- ¹A. J. Sievers and S. Takeno, *Phys. Rev. Lett.* **61**(8), 970–973 (1988).
- ²B. J. Page, *Phys. Rev. B* **41**(11), 7835–7838 (1990).
- ³P. Maniadis and S. Flach, *Europhys. Lett.* **74**(3), 452–458 (2006).
- ⁴A. J. Dick, B. Balachandran, and C. D. Mote, Jr., *Nonlinear Dyn.* **54**(1), 13–29 (2008).
- ⁵G. M. Chechin and G. S. Dzhelauhova, *J. Sound Vib.* **322**(3), 490–512 (2009).
- ⁶E. Kenig, B. A. Malomed, M. C. Cross, and R. Lifshitz, *Phys. Rev. E* **80**(4), 046202 (2009).
- ⁷M. Sato, N. Fujita, Y. Takao, S. Nishimura, W. Shi, Y. Sada, Y. Soga, and A. J. Sievers, *Nonlinear Theory Appl.* **3**, 87–102 (2012).
- ⁸U. T. Schwarz, L. Q. English, and A. J. Sievers, *Phys. Rev. Lett.* **83**(1), 223–226 (1999).
- ⁹M. Sato, B. E. Hubbard, L. Q. English, A. J. Sievers, B. Ilic, D. A. Czaplewski, and H. G. Craighead, *Chaos* **13**(2), 702–715 (2003).
- ¹⁰M. Kimura and T. Hikihara, *Phys. Lett. A* **373**(14), 1257–1260 (2009).
- ¹¹R. Stearrett and L. Q. English, *J. Phys. D: Appl. Phys.* **40**(17), 5394–5398 (2007).
- ¹²R. B. Thakur, L. Q. English, and A. J. Sievers, *J. Phys. D: Appl. Phys.* **41**(1), 015503 (2008).
- ¹³J. L. Ting and M. Peyrard, *Phys. Rev. E* **53**, 1011–1020 (1996).
- ¹⁴R. H. Austin, A. Xie, L. van der Meer, M. Shinn, and G. Neil, *J. Phys.: Condens. Matter* **15**, S1693–S1698 (2003).
- ¹⁵D. N. Christodoulides and R. I. Joseph, *Opt. Lett.* **13**, 794–796 (1988).
- ¹⁶M. Sato, B. E. Hubbard, and A. J. Sievers, *Rev. Mod. Phys.* **78**(1), 137–157 (2006).
- ¹⁷K. Forinash, M. Peyrard, and B. Malomed, *Phys. Rev. E* **49**(4), 3400–3411 (1994).
- ¹⁸S. Rakhmanova and D. L. Mills, *Phys. Rev. B* **58**(17), 11458–11464 (1998).
- ¹⁹L. De Marchi, E. Baravelli, M. Ruzzene, N. Speciale, and G. Masetti, *IEEE Trans. Ultrason., Ferroelectr., Freq. Control* **59**, 949–957 (2012).
- ²⁰H. Zhu and F. Semperlotti, *AIP Adv.* **3**, 092121 (2013).
- ²¹F. Casadei and M. Ruzzene, *Wave Motion* **49**, 605–616 (2012).
- ²²F. Semperlotti and H. Zhu, *J. Appl. Phys.* **116**, 054906 (2014).
- ²³C. Pierre, D. M. Tang, and E. H. Dowell, *Am. Inst. Aeronaut. Astronaut.* **25**(9), 1249–1257 (1987).
- ²⁴F. Georgiades, M. Peeters, G. Kerschen, J. C. Golinval, and M. Ruzzene, *Am. Inst. Aeronaut. Astronaut.* **47**(4), 1014–1025 (2009).
- ²⁵J. Cuevas, F. Palmero, J. F. R. Archilla, and F. R. Romero, *J. Phys. A: Math. Gen.* **35**(49), 10519–10530 (2002).
- ²⁶T. Rössler and J. B. Page, *Phys. Rev. B* **62**(17), 11460–11472 (2000).
- ²⁷B. P. Mann and N. D. Sims, *J. Sound Vib.* **319**, 515–530 (2009).
- ²⁸F. C. Moon and P. J. Holmes, *J. Sound Vib.* **65**, 275–296 (1979).
- ²⁹Z. Wu, R. L. Harne, and K. W. Wang, *J. Comput. Nonlinear Dyn.* **10**, 011016 (2014).